MRS Advances
https://doi.org/10.1557/s43580-023-00527-z

ORIGINAL PAPER

Pixelated carbon nanotube forests

Darian Smalley[1,2] · **Masa Ishigami**[1,2] · **R. E. Peale**[1,3]

Received: 28 November 2022 / Accepted: 16 February 2023

Abstract
Carbon nanotube forests (CNTFs) were grown on a patterned substrate to form square pixelated arrays. Two-level full factorial optimization first determined the best conditions for synthesis by chemical vapor deposition catalyzed by iron (Fe) nanoparticles deposited on oxidized silicon substrates. Varied parameters included growth temperature, growth time, and acetylene-to-hydrogen gas flow rate ratio. Argon was used as a carrier gas. Unpatterned CNTF heights were grown with values from 15.3 to 185.7 microns. Reactive ion etching of the substrate in oxygen plasma dramatically improved forest growth rates. Uniform square 7 × 7 pixel arrays were produced by contact photolithography and lift-off of the deposited Fe. Each pixel was subdivided into square islands separated by gaps with different island and gap dimensions, which ranged from 4 to 50 microns and 1 to 10 microns, respectively. The results demonstrate the fabrication of thermally and electrically isolated vertically aligned CNTF islands, which have applications to batteries, sensors, infrared absorbers, and infrared or electron emitters.

Introduction

Vertically aligned carbon nanotubes (CNT) forests (CNTF) have been reviewed in [1–3]. CNTFs are of interest for protein purification [4], batteries and supercapacitors [5, 6], sensors [7–9], and electron field emission devices [10, 11]. They are also useful as infrared absorbers and emitters since CNTFs can behave as almost perfect black bodies over the entire infrared spectrum [12].

Use of CNTs as infrared scene projectors (IRSP) for hardware-in-the-loop testing of IR imagers was suggested in [13]. Specific CNTF-based infrared scene projectors with optical heating was proposed in [14]. Initial investigations (Joe LaVeigne, Santa Barbara Infrared Inc., private communication) revealed that lateral heat diffusion degrades the spatial resolution and maximum apparent radiant temperature. A suggested solution is to disrupt that heat diffusion with "fire-breaks," i.e., patterned gaps that divide CNTFs into thermally isolated islands [15]. This paper explores the fabrication of such patterned CNTF nanostructures for application to IRSP. The novelty of our present work is that our optimized growth method yields patterned CNTF with achieved pitch smaller than previous efforts. Furthermore, our method does not require the use of an aluminum oxide catalyst support layer [16, 17].

Experimental

Oxidized silicon wafers from University Wafer were quartered and used as substrates. Reactive ion etching (RIE) of the SiO_2 substrate with oxygen plasma was accomplished with 50 watts of power for 3 min at a pressure of 53 mTorr. About 1 nm of Fe was electron beam evaporated onto the silicon oxide surface as the catalyst layer. Carbon nanotube growth was performed in a quartz tube within a Thermo Scientific Lindberg/Blue M furnace. An anneal step (30 s in H_2/Ar) occurs inside the tube furnace to condense the Fe film into nanodots. Then acetylene was added to the gas mix as the carbon source for CNTF growth.

During initial growths, it was observed that the tallest CNTFs with the straightest vertical alignment grew near cleaved substrate edges and on scratches. Reasoning that fresh surfaces devoid of contaminants are important for growth, we were motivated to condition the surfaces by RIE.

✉ R. E. Peale
Robert.peale@ucf.edu

[1] Department of Physics, University of Central Florida, Orlando, FL 32816, USA

[2] Nanoscience Center, University of Central Florida, Orlando, FL 32816, USA

[3] Truventic LLC, 1209 W. Gore St., Orlando, FL 32805, USA

Published online: 28 February 2023

Any achieved roughening was unmeasurable by atomic force microscopy.

A two-level full factorial experiment optimized growth parameters [18]. The chosen parameters were growth temperature, growth time, and reaction gas flow ratio (acetylene:hydrogen). Each factor was assigned high and low values, chosen based on CNTF literature. The values were 780 or 900 °C, 3 or 10 min, and 0.28 or 0.06 ratio, respectively. The high and low flow rates of the acetylene were 60 sccm and 20 sccm, while the high and low flow rates of the hydrogen were 1000 sccm and 70 sccm. This resulted in 8 trials, the order of which was randomized. A mid-point value for the 3 parameters was added to the experiment to seek non-linearity in the response, which was chosen to be the CNTF height. Qualitative factors such as vertical alignment and uniformity were also noted. Scanning electron microscopy (SEM) was used to characterize forest coverage, alignment, and maximum height of each sample. No attempt was made to characterize the number of walls within each nanotube.

Once the growth conditions were optimized, we proceeded to patterned growth. A photomask of four identical pixel arrays was used to produce patterned CNTFs. Each 7×7 array comprised 49 pixels of 2 mm×2 mm dimensions. Each pixel was subdivided into square islands separated by gaps. Island and gap dimensions were different in each pixel. The island dimensions were 4, 10, 15, 20, 30, 40, or 50 µm. The gaps between islands were 1, 2, 3, 4, 6, 8, or 10 µm. All combinations of island and gap sizes were produced to make up the 49 pixels in the array. The patterns were produced by conventional contact photolithography on three-inch wafers, resulting in 4 identical arrays per wafer. Each set of arrays patterned in Shipley 1813 photoresist was metalized with iron as described above, followed by lift-off in Remover PG. They were then rinsed with isopropanol followed by water to produce the patterned catalyst. All patterned CNTFs were grown in these arrays using optimized parameter values to target a maximum forest height of 150 µm. This height was chosen, a priori, as a compromise between absorptivity/emissivity and heat dissipation into the substrate in order to disrupt lateral heat diffusion across the forest, as motivated by the application to IRSP.

Results

Detailed plots and analysis of the full factorial experiments will be presented elsewhere (D. Smalley, PhD dissertation, University of Central Florida). We summarize the findings in Table S1 (Supplemental Information). Surface plots were prepared, e.g., of CNTF height vs. temperature and flow rate. Fits assumed a model that was linear in the main and interaction effects. A mid-point trial revealed non-linearity between growth time and flow ratio on the CNTF height.

The main effect of a given factor is a measure of how the response changed as the factor changed, while other factors are kept constant. It is the difference between the average responses at the low and high levels of the considered factor. This can be visualized by fitting a line to the points on a plot of response vs. the considered factor. A higher slope indicates that the considered factor is responsible for more change to the response than other factors that give lower slope. We find that temperature as a factor has a large positive main effect and is responsible for 39% of the variation. The positive sign associated with the main effect of the growth temperature factor indicates that forest height increases with increasing temperature.

When the effect of one factor on the response depends on the level of another factor, they are said to *interact*. This interaction effect can be quantified by the difference between the effect of one factor at the high and low levels of the other factor. Interaction effects can be visualized by plotting the response averaged over each level of one of the factors, for each level of the second factor. This results in two lines, one for each level of the second factor. Similar slopes for both lines indicate little interaction. Dissimilar slopes or intersecting lines suggest strong interaction between the two factors. From such analysis, we found strong interaction between flow ratio and growth time. The interaction effect between these two factors is responsible for an additional 39% of the observed variation in response. When growth time is long (short), low (high) flow ratio is favored. This is consistent with other studies [4].

An ordered bar chart of contribution to response variation for the main and interaction effects is called a Pareto plot. Our Pareto plot shows that the main effect of growth temperature and the interaction effect of growth time and flow ratio contribute 78% to the total maximum height response. Thus, these are the most important factors to control when optimizing for maximum CNTF height. The optimized parameter values determined by the analysis are growth temperature = 840 °C, growth time = 6.5 min, and flow ratio = 0.06. Subsequent growths under these conditions produced pixelated CNTF samples with uniform heights of 150 µm and low tortuosity. These interpretations and optimal values agree with results of similar studies on CNTF yield [4, 19–21].

Figure 1 (left) presents an SEM image of the tallest unpatterned CNTF growth achieved, with a maximum height of 2.5 mm. While millimeter-scale forest height was not the focus of this work and instead was a preliminary result, the growth conditions and plasma treatment leading to it were replicated and observed to reproduce such growth. A control sample included with the replication which was not exposed to O_2 RIE did not display any millimeter-scale growth, as shown in Fig.

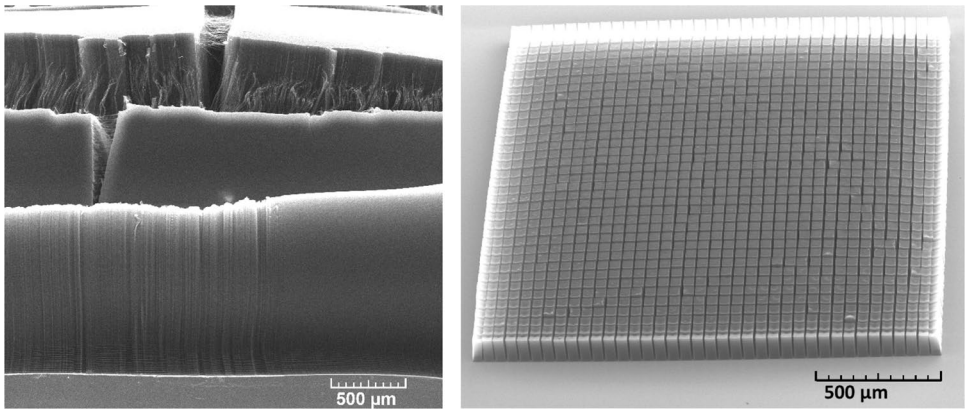

Fig. 1 (left) SEM image of 2.5-mm tall unpatterned CNTF profile. (right) Carbon nanotube forest subdivided into islands separated by gaps

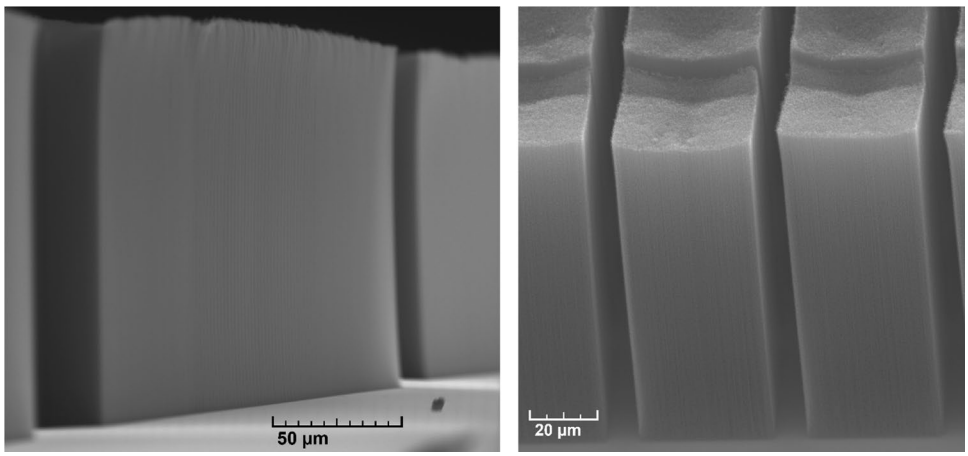

Fig. 2 SEM images of array subdivision detail in a CNTF pixel

S1 found in the supplemental information. Height was subsequently controlled by adjusting the growth duration. Figure 1 (right) presents an image of one of the 2 mm × 2 mm pixels in the 49-pixel array. This pixel is subdivided into square islands separated by gaps where very few of the islands are touching.

Figure 2 presents higher magnification images of islands within the pixel of Fig. 1. The CNTFs have low tortuosity and are highly vertically aligned. In Fig. 2 (left) the CNTF height is 150 µm. Figure 2 (right) shows well-defined islands with widths of 40 µm separated by 10-µm gaps.

Figure 3 presents a close-up SEM image within one of the CNTF islands within one pixel. A high level of alignment is seen where nearly all nanotubes are parallel with low tortuosity. We have found that island sizes below 15 micron produce poor results, while we do not see any relationships between CNTFs and morphology of CNTs. Our results can be found in Table S2 (Supplementary information).

Discussion and summary

RIE of the SiO_2 substrate in O_2 plasma before depositing the Fe catalyst dramatically increased the CNTF alignment and growth rate. Under the same growth conditions, the

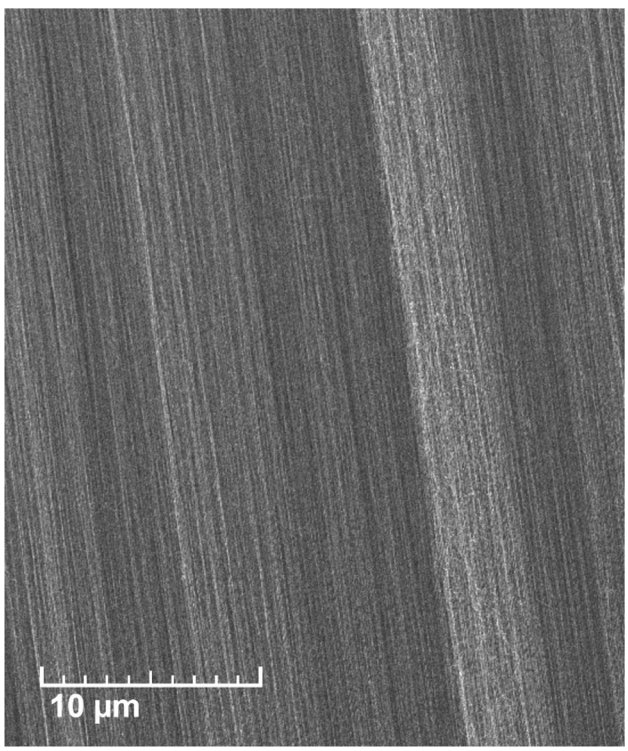

Fig. 3 SEM image of vertically aligned CNTFs

RIE treatment increased the CNTF height from 185 µm to 2.5 mm, which corresponds to nearly 14 times growth rate increase, to 0.25 mm/min. We have been unable to find mention of such an RIE step in previous CNTF literature. Roughening a silicon substrate surface by anodization before Fe deposition has been shown to improve growth rate [10], and this was explained by improved flow of reaction gas to the catalyst particles at the base. However, the CNTFs displayed comparatively high tortuosity and showed an average growth rate of only 6 µm/min. As such, we conclude the growth enhancement by the RIE step is not due to increased roughness. Instead, we suspect that the formation of the iron oxide catalyst during the annealing step is enhanced by oxygen on the top surface [22]. RIE offers a cleaner process, which is more compatible with wafer processing.

Patterning of CNTFs was achieved here by conventional contact photolithography and lift-off of the evaporated Fe catalyst. This allowed sharp-edged gaps as small as a few microns between islands that were 150 µm tall and which had high vertical alignment and low tortuosity. Patterning has been achieved previously by depositing Fe through a shadow mask [10] and by patterned formation of nanoparticles in a catalyst film by laser melting [23]. It is also possible to deposit a patterned promotion or inhibition layer on top of the catalyst [24], but CNTs tend to grow underneath the patterned inhibitor. Other methods of patterning were reviewed in [1], but the resulting CNTFs had lower quality. Conventional lift-off, as presented here, should be better at achieving small gap dimensions with sharp transitions while maintaining high CNTF fill factor, as needed to control lateral heat diffusion for the IRSP application.

Supplementary Information The online version contains supplementary material available at https://doi.org/10.1557/s43580-023-00527-z.

Acknowledgments This work was supported by Santa Barbara Infrared Inc.

Data availability Data are available from the authors upon reasonable request.

Declarations

Conflict of interest R. E. Peale has ownership in Truventic LLC and may benefit financially from the results of this research. Otherwise, all authors certify that they have no affiliations with or involvement in any organization or entity with any financial interest or non-financial interest in the subject matter or materials discussed in this manuscript.

References

1. H. Chen, A. Roy, J.-B. Baek, L. Zhu, J. Qu, Mater. Sci. Eng. R **70**, 63 (2010). https://doi.org/10.1016/j.mser.2010.06.003
2. J.-Q. Huang, Q. Zhang, M.-Q. Zhao, F. Wei, Chin. Sci. Bull. **57**, 157 (2012). https://doi.org/10.1007/s11434-011-4879-z
3. E.G. Rakov, Russ. Chem. Rev. **82**, 538 (2013). https://doi.org/10.1070/RC2013v082n06ABEH004340
4. N.M. Mubarak, F. Yusof, M.F. Alkhatib, Chem. Eng. J. **168**, 461 (2011). https://doi.org/10.1016/j.cej.2011.01.045
5. R. Lin, P.-L. Taberna, S. Fantini, V. Presser, C.R. Perez, F. Malbosc, N.L. Rupesinghe, K.B.K. Teo, Y. Gogotsi, P. Simon, J. Phys. Chem. Lett. **2**, 2396 (2011). https://doi.org/10.1021/jz201065t
6. L. Yu, G.Z. Chen, Front. Chem. (2019). https://doi.org/10.3389/fchem.2019.00272
7. S. Chun, W. Son, C. Choi, Carbon **139**, 586 (2018). https://doi.org/10.1016/j.carbon.2018.07.005
8. P.R. Mudimela, M. Scardamaglia, O. Gonzalez-Leon, N. Reckinger, R. Snyders, E. Llobet, C. Bittencourt, J.F. Colomer, Beilstein J. Nanotechnology **5**, 910 (2014). https://doi.org/10.3762/bjnano.5.104
9. Z. Zhu, L. Garcia-Gancedo, C. Chen, X.R. Zhu, H.Q. Xie, A.J. Flewitt, W.I. Milne, Sens. Actuators B-Chem. **178**, 586 (2013). https://doi.org/10.1016/j.snb.2012.12.112
10. S. Fan, M. Chapline, N.R. Franklin, T.W. Tombler, A.M. Cassell, H. Dai, Science **283**, 512 (1999). https://doi.org/10.1126/science.283.5401.512
11. M.O. Hassan, A. Nojeh, K. Takahata, ACS Appl. Nano Mater. **2**, 4594 (2019). https://doi.org/10.1021/acsanm.9b00948
12. A.M. Gheitaghy, A. Ghaderib, S. Vollebregta, M. Ahmadic, R. Wolffenbuttel, G.Q. Zhang, Materials Res. Bull. **126**, 110821 (2020). https://doi.org/10.1016/j.materresbull.2020.110821
13. W. R. Owens, D. L. Barker, US patent 9241115, Jan 19, 2016.
14. R. Fainchtein, D. M. Brown, C. C. Davis, US Patent 20130048884 A1 February 28, 2013).
15. J. D. LaVeigne, G. P. Matis, T. E. Danielson, US Patent 20220256654 A1, August 11, 2022.
16. Y. Hayamizu, T. Yamada, K. Mizuno et al., Nature Nanotech. **3**, 289–294 (2008). https://doi.org/10.1038/nnano.2008.98
17. M.F.L. De Volder et al., J. Micromech. Microeng. **21**, 045033 (2011). https://doi.org/10.1088/0960-1317/21/4/045033
18. G.E.P. Box, W.G. Hunter, S.J. Hunter, *Statistics for Experimenters* (Wiley, New York, 1978)
19. I. Willems, Z. Kónya, J.-F. Colomer, G. Van Tendeloo, N. Nagaraju, A. Fonseca, J.B. Nagy, Chem. Phys. Lett. **317**, 71 (2000). https://doi.org/10.1063/1.1342509
20. T. Ikuno, J.-T. Ryu, T. Oyama, S. Ohkura, Y.G. Baek, S. Honda, M. Katayama, T. Hirao, K. Oura, Vacuum **66**, 341 (2002). https://doi.org/10.1016/S0042-207X(02)00141-0
21. R.G. Lacerda, A.S. The, M.H. Yang, K.B.K. Teo, N.L. Rupesinghe, S.H. Dalal, K.K.K. Koziol, D. Roy, G.A.J. Amaratunga, W.I. Milne, M. Chhowalla, D.G. Hasko, F. Wyczisk, P. Legagneux, Appl. Phys. Lett. **84**, 269 (2004). https://doi.org/10.1063/1.1639509
22. A.K. Mahapatro, A. Scott, A. Manning, D.B. Janes, Appl. Phys. Lett. **88**, 151917 (2006). https://doi.org/10.1063/1.2183820
23. M. Terrones, N. Grobert, J. Olivares, J.P. Zhang, H. Terrones, K. Kordatos, W.K. Hsu, J.P. Hare, P.D. Townsend, K. Prassides, A.K. Cheetham, H.W. Kroto, D.R.M. Walton, Nature **388**, 52 (1997). https://doi.org/10.1038/40369
24. J.Q. Huang, Q. Zhang, M.Q. Zhao, G.-H. Xu, F. Wei, Nanoscale **2**, 1401 (2010). https://doi.org/10.1039/c0nr00203h